4. RELAXATION OF P@C_{60}

Each quantum mechanical system is sensitive to its environment. When it is driven away from thermal equilibrium, the interaction with the environment tends to restore the initial state. This process is called relaxation or decoherence. Any quantum computer should have long relaxation times, which means that the time needed to perform logic gates must be much shorter than the decoherence time. At the beginning of the development of quantum information processing (QIP) theory it was thought that decoherence is so fast that it will hinder the physical implementation of QIP, but after invention of the quantum error correction (QEC) this problem could be overcome. QEC codes use ancillary qubits to store quantum information which reduces the error in computation.
The relaxation properties of "bulk" (diluted in polycrystalline C_{60}) P@C_{60} and of a single crystal of P@C_{60} in BrPOT are presented in this chapter. First the general theory of relaxation will be shortly reviewed.

4.1 Theoretical Background

The general theory of relaxation was first developed by Bloch [89] and later generalized by Redfield [90, 91], who introduced an additional term to the Liouville-von Neumann equation (1.27) to include relaxation. The resulting "master equation" is written like:

$$\frac{d\rho(t)}{dt} = -i[\mathscr{H}(t), \rho(t)] + \mathscr{R}(\rho(t) - \rho(\infty)) \tag{4.1}$$

where $\mathscr{H}$ is the Hamiltonian of the system, $\mathscr{R}$ is the relaxation matrix, $\rho(t)$ is the density matrix at time t and $\rho(\infty)$ at equilibrium. The relaxation matrix $\mathscr{R}$ connects every element of the density matrix with all other elements and accordingly $\mathscr{R}$ has dimension n^4. Its matrix elements are:

$$R_{abcd} = J_{acbd}(\omega_{ac}) + J_{acbd}(\omega_{db}) - \delta_{ac}\sum_e J_{ebed}(\omega_{be}) - \delta_{bd}\sum_e J_{ecea}(\omega_{ea}) \tag{4.2}$$

The spectral density J is defined as:

$$J_{abcd}(\omega) = \int_0^\infty \overline{\langle a|\mathscr{H}'(t)|b\rangle\langle c|\mathscr{H}'(t+\tau)|d\rangle^*}\exp(i\omega\tau)d\tau$$

$\mathscr{H}'(t)$ is the time dependent part of the Hamiltonian responsible for relaxation, ω is the observation frequency. The bar above the matrix element denotes an ensemble average. Redfield's master equation is quite general and can be used for a large variety of decoherence processes, not only in magnetic resonance where it was first used. Solving this system of coupled differential equations is a very difficult task, but fortunately it is not necessary for most cases.

Usually the earlier theory of Felix Bloch [89], originally written for an ensemble of nuclear spins, is used for the description of relaxation in magnetic resonance. Consider a large number of electron spins in a magnetic field. Their motion can described by the classical equation of motion to which phenomenologically a relaxation term is added:

$$\frac{M_z}{dt} = \gamma(\mathbf{B} \times \mathbf{M})_z + \frac{M_0 - M_z}{T_1} \tag{4.3}$$

$$\frac{M_x}{dt} = \gamma(\mathbf{B} \times \mathbf{M})_x - \frac{M_x}{T_2} \tag{4.4}$$

$$\frac{M_y}{dt} = \gamma(\mathbf{B} \times \mathbf{M})_y - \frac{M_y}{T_2} \tag{4.5}$$

here $\mathbf{M} = (M_x, M_y, M_z)$ is the net magnetization vector of the ensemble, M_0 is its equilibrium value and $\gamma = g\mu_B/\hbar$ is the gyromagnetic ratio for electron spins. There are two relaxation times defined - T_1 for spin-lattice (or longitudinal) relaxation and T_2 for spin-spin (or transverse) relaxation. When a short MW pulse is applied to the system and it is left to evolve under the constant applied magnetic field then T_1 tends to restore the z component of the magnetization to its equilibrium value M_0 ($M_z \sim M_0(1 - ce^{-\frac{t}{T_1}})$), while T_2 is responsible for the decay of the x and y components of M ($M_{x,y} \sim e^{-\frac{t}{T_2}}$). In the language of quantum mechanics, T_1 affects the diagonal components of the density matrix and restores them to their thermal equilibrium value, while T_2, sometimes called coherence time, accounts for the decay of the off-diagonal components of ρ. Normally $T_1 \geq T_2$.

In certain cases the relaxation times T_1 and T_2 from the Bloch equations can be calculated analytically from the more general Redfield theory.

4.2 Spin-Lattice Relaxation

Knowing T_1 and how it depends on the temperature is very important for the design of a quantum computational experiment since T_1 limits the length of any pulse sequence. However, after an experiment is done (for example one point of a echo decay), the system should relax to its initial state and then the next "shot" can be done. The delay time is called shot repetition time and must be longer than $5T_1$.

Thus if T_1 is too long, each measurement will take too much time, and a temperature with optimal T_1 must be found for each experiment.
The relaxation properties of group V endohedral fullerenes were already investigated in a number of studies [92, 93, 94, 47, 95]. The spin-lattice relaxation was measured using the inversion recovery pulse sequence (chapter 1) for different temperatures. There are two proposed mechanisms which cause the relaxation in N@C_{60} and P@C_{60} - fluctuation in the fine structure and fluctuation of the hyperfine interaction [93, 94, 47] corresponding to the two different relaxation rates R_{hf} and R_{fs}. The possible relaxation pathways are depicted in Fig. 4.1. Two longitudinal relaxation times

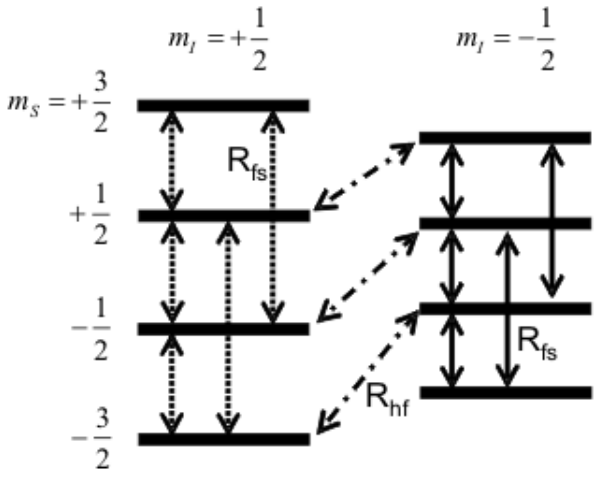

Fig. 4.1: Relaxation pathways due to fluctuations of the fine R_{fs} and hyperfine R_{hf} structure interaction in a system with electron spin $S = 3/2$ and nuclear spin $I = 1/2$ [94]

$R_{hf} = 1/T_1^a$ and $R_{fs} = 1/T_1^b$ are defined and relaxation of the magnetization is written as:

$$m_z(t) = 1 - 2f(t) = 1 - 2f_{hf}(t)f_{fs}(t) \tag{4.6}$$

where $f_{hf}(t)$ and $f_{hf}(t)$ are the relaxation functions depending on fluctuations of the hyperfine and fine structures respectively [94, 47]:

$$f_{hf}(t) = \frac{1}{40}\left[29 + 10e^{-\frac{3}{2}R_{hf}(T)t} + e^{-2R_{hf}(T)t}\right] \tag{4.7}$$

$$f_{fs}(t) = e^{-\frac{9}{5}R_{fs}(T)t} \tag{4.8}$$

The endohedral atom in the fullerene cage is situated in a three dimensional potential and behaves like a harmonic oscillator [96, 51, 92] introducing fluctuations in the hyperfine coupling constant a as well as in the ZFS constant D. The former is considered to be the main relaxation mechanism in P@$_{60}$ [47].
The recovery of the magnetization of both polycrystalline P@C_{60} and P@C_{60} in

BrPOT is best described by a double exponential function. The two relaxation times T_1^a and T_1^b for the "bulk" endohedrals are generally longer as in the endohedrals in the solid state matrix possibly due to the neighboring protons in the latter. In "bulk" P@C_{60} a mean relaxation rate was defined as $R_{mean} = 1/T_1^a + 1/T_1^b$ and it is determined by the fluctuations of the hyperfine constant:

$$R_{mean} \approx \Delta a^2 \tag{4.9}$$

where $\Delta a^2(T) = (a(T)/2\pi h - a_0/2\pi h)^2$. The comparison of $R_{mean}(T)$ and $\Delta a^2(T)$ shows good agreement, suggesting that the fluctuations in the hyperfine structure are a major relaxation pathway. In P@C_{60} in BrPOT there are also two relaxation rates but their temperature dependence shown in Fig. 4.2 is different from P@C_{60} shown in Fig. 4.3. In Fig. 4.2 (left) is the temperature dependence of T_1^a, T_1^b is

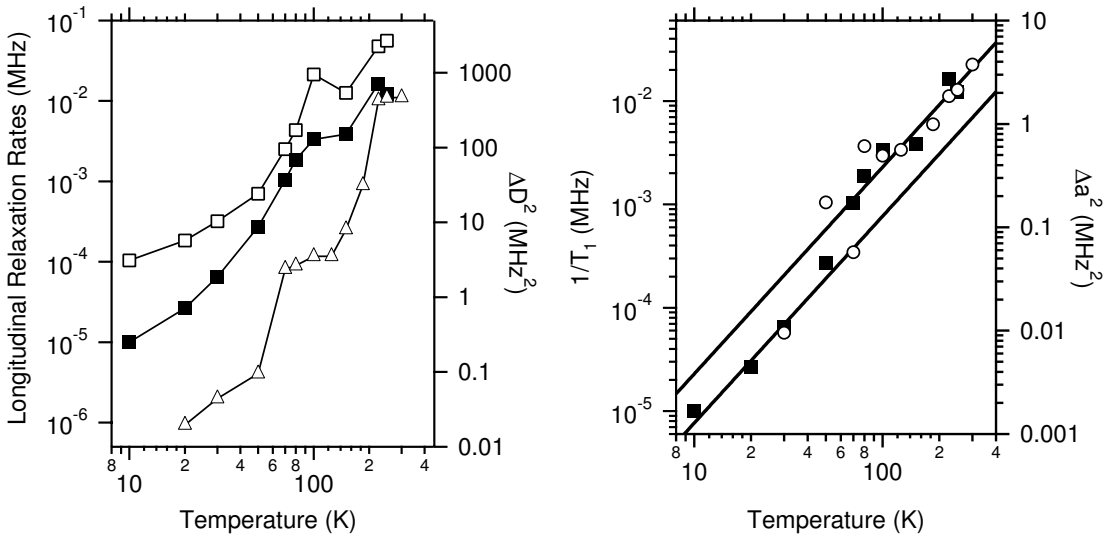

Fig. 4.2: Temperature dependence of the longitudinal relaxation rates $1/T_1^a$ (filled squares) and $1/T_1^b$ (open squares) of P@C_{60} in rhombohedral BrPOT. Open triangles denote the change of the ZFS $\Delta D^2(T) = (D(T) - D_0)^2$ (left graph) and open circles denote the change in the hyperfine constant $(\Delta a)^2 = (a(T) - a_0)^2$ where D_0 and a_0 denote correspondingly the values for D and a at the lowest temperature. The two solid lines in the right graph fit the relaxation rate to a function $f(T) \approx 1/T^2$. All other lines connect the data points.

shown together with the change of the ZFS defined as $\Delta D^2(T) = (D(T) - D_0)^2$ where D_0 is the value of ZFS as the lowest temperature. From the plot it can be seen that there are three different temperature regions. At low temperatures $1/T_1^a$ and $1/T_1^b$ strongly increase up to $T = 50$ K where a jump in the ZFS occurs. For temperatures between 50 and 200 K the relaxation rates show stronger temperature dependence, which changes again when the size of the ZFS makes a jump at $T \sim 210$ K. Above $T = 210$ K, ΔD, $1/T_1^a$ and $1/T_1^b$ show somehow weaker temperature dependence. It

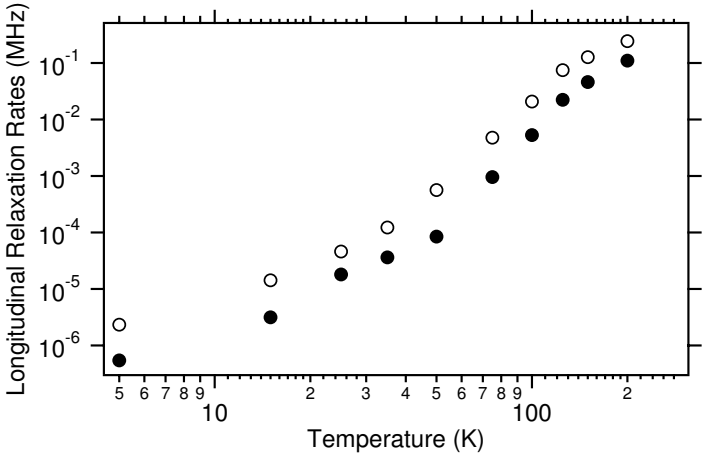

Fig. 4.3: Temperature dependence of the longitudinal relaxation rates $1/T_1^a$ (filled squares) and $1/T_1^b$ (open squares) of polycrystalline P@C_{60} (adapted from [47])

is thus clear that the ZFS influences the spin-lattice relaxation. In the right graph in Fig. 4.2 the relaxation rate $1/T_1^b$ is plotted together with the change of the hyperfine constant written as $(\Delta a)^2 = (a(T) - a_0)^2$ as a function of temperature. The two solid lines fit $f(T) \approx 1/T^2$ to the relaxation rate in two temperature regions - one is T below $T = 50$ K and the other is above 50 K where the fit is better. Such a temperature dependence is expected from the theory for Raman processes in the high temperature limit $T \gg T_D$ where T_D is the Debye temperature [82]. This process for spin-lattice relaxation consists of an absorbtion of a phonon with frequency ω_a, flip of the electron spin and release of a phonon with another frequency ω_b. T_D can be calculated using the formula [97]:

$$T_D = \frac{\hbar c_{snd}}{k}\left(\frac{6\pi^2 N_{cell}}{V_{cell}}\right) \tag{4.10}$$

where c_{snd} is the sound velocity in the material, N_{cell} is the number of atoms per unit cell with volume V_{cell}. For rhombohedral BrPOT $T_D = 0.13 c_{snd}$ and if the velocity of sound in the fullerenes is substituted in the formula then $T_D = 272.4$ K. Therefore the observed the spin-lattice relaxation cannot be caused by a Raman process and possibly there are other processes which take part.

In the BrPOT encapsulated fullerenes longitudinal relaxation was measured on transitions with $m_S = +3/2 \leftrightarrow m_S = +1/2$ ($m_S = -1/2 \leftrightarrow m_S = +3/2$) and $m_S = +1/2 \leftrightarrow m_S = -1/2$ selectively and no significant difference was found within the experimental error. This result suggests that the fluctuations of the fine structure are not the main relaxation pathway similar to the "bulk" P@C_{60}. Thus the reduced values of the T_1 for P@C_{60} in BrPOT are possibly due to coupling to the abundant protons from the solid state matrix.

4.3 Spin-Spin Relaxation

The spin-spin relaxation time T_2 is the time scale at which the off-diagonal components of the density matrix decay, i.e. the coherence between different energy levels decays. Accordingly, T_2 is the upper time limit for coherent operation of a quantum computer (QC), or just the time during which the computer works. If T_2 is divided by the gate time, the longest time needed to perform an operation on qubits, the theoretical maximum number of gate operations N_{gate} is obtained before the QC needs to be restarted. Certainly there will be some delays between the gates, so the theoretical N_{gate} will never be reached, yet it must be as large as possible and it serves as an indication of the potential of a particular QC implementation. For a good quantum computer a long T_2 is needed so the relaxation processes should be well understood in order to control the decoherence and thus to achieve maximal operation time.

The transverse relaxation time T_2 is usually measured with a Hahn echo pulse sequence (chapter 1). The distance between the two MW pulses is increased and a decay of the magnitude of the electron spin echo (ESE) is measured. This method was initially introduced for NMR by Hahn [42]. This method only yields the phase memory time T_m is obtained, in the literature often associated with the "natural" T_2 [98, 39]. Carr and Purcell discovered later that in the presence of diffusion in the sample the Hahn echo pulse sequence must be modified in order to measure the real T_2 [99]. They distinguished two different T_2 times, calling the Hahn echo "method A" and proposed a new pulse sequence to measure the real T_2 - method B [99]. The experiment shown in Fig. 4.4 begins with a $\pi/2$ pulse applied along the

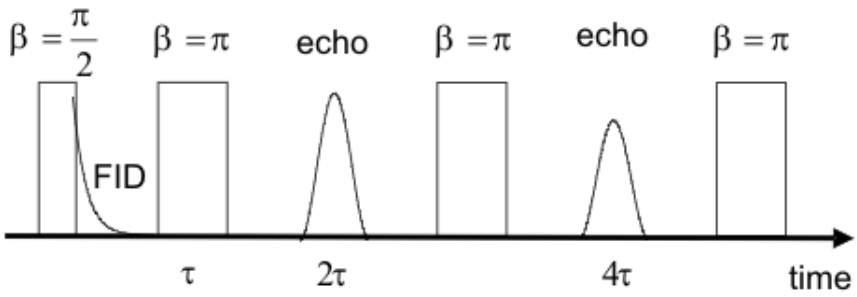

Fig. 4.4: Carr-Purcell-Meiboom-Gill (CPMG) pulse sequence for measuring T_2.

x axis in the rotating frame, which rotates the initial magnetization to the y axis. This is followed by a pulse train of π pulses along the same axis. It was found that the results of this experiment are very sensitive to the amplitude of the π pulses

and later Meiboom and Gill modified the pulse sequence by applying the π pulse along the y axis [100]. As $T_2 > T_m$, the condition $\tau \gg T_m$ must be fulfilled in order to measure T_2 accurately. The method was developed first for NMR and is now known as the Carr-Purcell-Meiboom-Gill (CPMG) pulse sequence. Later on other multi pulse were techniques designed [101, 102, 103] consisting of repeated cycles of pulses. They are widely used to obtain additional information about the spin system, for example to decouple them from each other and to reduce the line width (increase the T_m). Recently, a modified decoupling sequence was used to decouple the ^{29}Si nuclear spins from each other, thus increasing the T_m by several orders of magnitude [104].

The application of CPMG and other decoupling techniques in ESR experiments is not straightforward since the MW electronics is less well developed. For many solid state ESR samples, T_m is at most of the order of microseconds and in order to fulfill $\tau/T_2 \ll 1$, τ must be rather short. The main obstacle is that the standard pulse ESR (X band) spectrometers are usually equipped with traveling wave tube (TWT) amplifiers with about 1 kW output power in order to manage short enough pulses (and thus broad spectral excitation), but these cannot work continuously. Typically a TWT has to be used not more than about 1 % of the time (duty cycle), otherwise it can be damaged. There are other types of spectrometers that can be used to circumvent the problem [105], but only samples with quite long T_m can then be used.

The magnetic dipolar interaction between the electron spins under study is usually the main processes that contributes to the spin-spin relaxation. One can define two types of spins - A and B [39, 106, 107]. The former are excited by the MW pulse while the latter are undisturbed. After the A spins are excited, part of their magnetization is transferred to the B spins through dipolar interaction and some of the equilibrium magnetization is transferred back from the B to the A spins. Random flips of the B spins can also cause decay of the magnetization. As a result there is an extraneous contribution to the relaxation of the A spins, called spectral diffusion. For this process the following expression is given for T_m [108]:

$$T_m = 1.4\sqrt{\frac{4\pi\hbar T_1^{(B)}}{2.53\mu_0 g_A g_B \mu_B^2 C_B}} \tag{4.11}$$

where $T_1^{(B)}$ is the spin-lattice relaxation time of the B spins and C_B is their concentration. Another possibility for relaxation of the non-equilibrium magnetization in the A spins is the interaction among them. A MW pulse excites (flips) the A spins, which leads to a change of the local field at each particular A spin. These flips induce relaxation, a process called instantaneous diffusion [106, 109]. The contribution of

latter to the relaxation is described by the following expression [106]:

$$\frac{1}{T_{ID}} = \frac{8\pi^2}{9\sqrt{3}\hbar} g^2 \mu_B^2 C_A \langle \sin^2(\frac{\theta}{2}) \rangle \tau \tag{4.12}$$

where C_A is the A-spin concentration and θ is the rotation angle of the second pulse in the Hahn echo sequence. In order to test experimentally if instantaneous diffusion is a major relaxation process, the ESE signal decay should be recorded for different θ and then $1/T_{ID}$ should follow equation (4.12). There are several studies confirming the validity of equation (4.12) for different systems [110, 111].

After this brief review of the basic spin-spin relaxation mechanism we note that the CPMG pulse sequence refocuses dipolar interactions between resonant and non-resonant electron spins, i.e. spectral diffusion, which is analogous to heteronuclear interaction in NMR [105, 101]. It does not refocus dipolar interaction between resonant spins, i.e. instant diffusion. Thus contributions from instant diffusion to the relaxation will not be refocused, in contrast to the spectral diffusion.

The complete isolation of the endohedral atom in N@C_{60} and P@C_{60} from its environment suggests that diluted samples would have long spin-spin relaxation times which was confirmed experimentally [92, 49]. When the spin concentration (m(N@C_{60})/m(C_{60})) is increased, an increase in the line width is observed corresponding to a reduced transverse relaxation time[92]. This effect is expected as the magnetic dipolar interaction grows as $\sim 1/r^3$, where r is the distance between the spins. Similar experiments were done for P donors in silicon, where below a certain spin concentration T_2 is constant [112].

Several polycrystalline samples of P@C_{60} diluted in C_{60} were prepared down to the lowest measurable spin concentration of 10^{-8} (10^{13} spins/cm^3). T_m and T_2 were measured with Hahn echo and CPMG pulse sequence respectively. A typical time trace for the ESE decay is shown in Fig. 4.5 (top) and CPMG in Fig. 4.5 (bottom). Time traces for all of the samples (measured with Hahn echo and CPMG) were fitted with a single exponential function. When the two methods are compared it is clear that with help of the CPMG pulse sequence the transverse magnetization is preserved for a longer time than with the Hahn echo (see table 4.1). It must be noted that T_2 values measured by CPMG pulse sequence are only lowest estimates due to the limited number of MW pulses. The used Bruker X-band ESR spectrometer E600 has a hardware limit of 32 pulses. T_m (T_2) is determined only by the magnetic dipolar interaction between the endohedral fullerenes, thus no temperature dependence is expected. Fig. 4.6 shows the relaxation rates $1/T_m$ for "bulk" P@C_{60} at different temperatures measured in X-Band by ESE decay. Around room temperature $T_m \approx 2T_1$ thus T_1 limits T_m in that temperature region. An increase

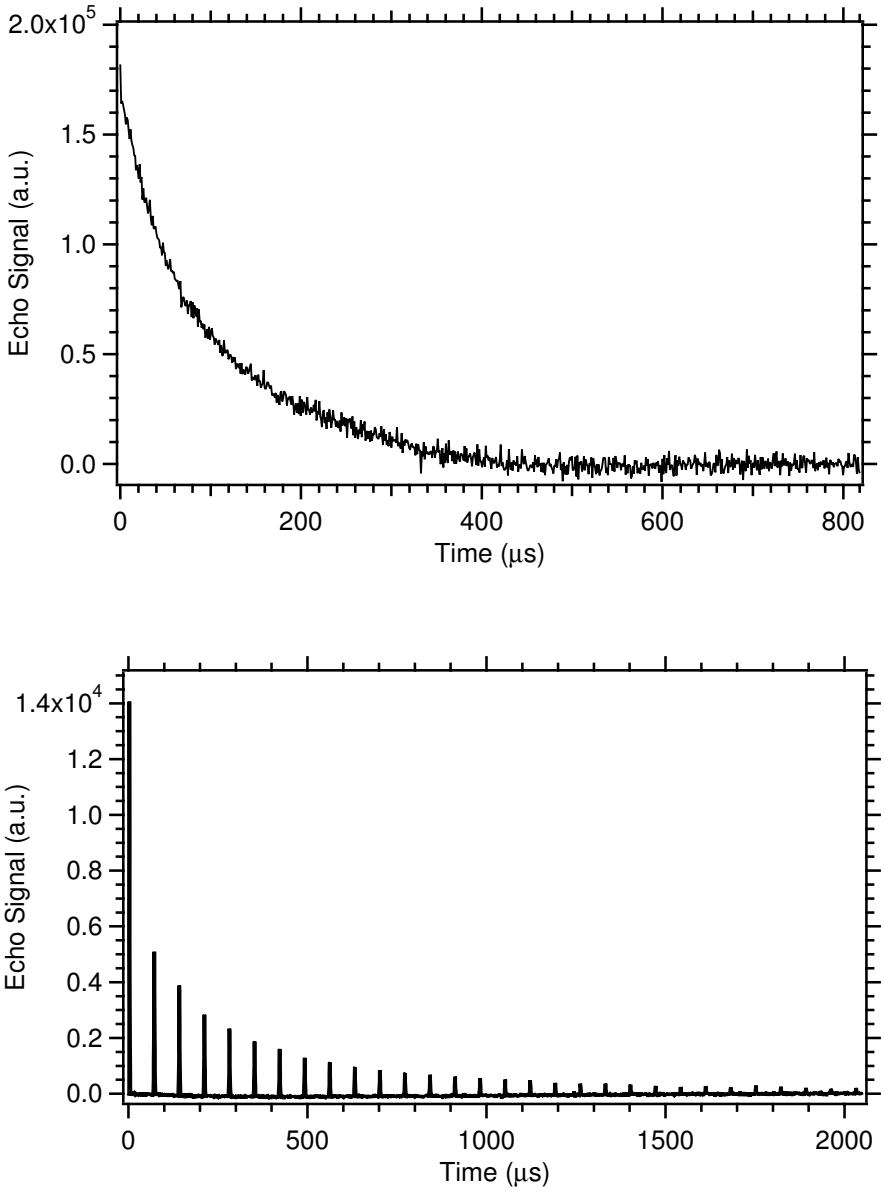

Fig. 4.5: Time traces of the ESE decay (top) and of the CPMG pulse sequence (bottom) in polycrystalline P@C_{60}.

Spin concentration (g/cm^{-3})	T_m (μs), ESE decay	T_2 (μs), CPMG
2.0×10^{15}	11.2	11.1
6.3×10^{14}	68.7	151.6
1.9×10^{14}	106.5	287.5
6.3×10^{13}	113.25	416.6

Tab. 4.1: Spin-spin relaxation for magnetically diluted polycrystalline samples P@C_{60} at $T = 10$ K measured with ESE decay and CPMG pulse sequences.

in T_m is observed as the temperature is lowered, but not as strong as by T_1, and T_m is constant below 40 K in contrast to T_1.

The data for $1/T_m$ and $1/T_2$ of polycrystalline P@C_{60} samples with different spin

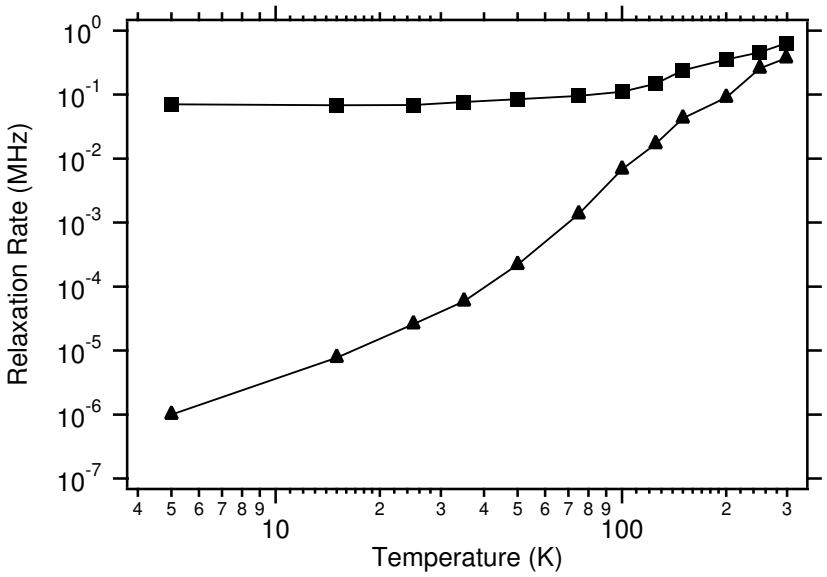

Fig. 4.6: Temperature dependence of the mean spin-lattice (triangles) and spin-spin relaxation (squares) rates of polycrystalline P@C_{60} (adapted from [47]).

concentrations measured with ESE decay and the CPMG pulse sequence are plotted in Fig. 4.7 and listed in table 4.1. The solid lines are exponential function which fit $1/T_m$ and $1/T_2$ experimental data points. From the figure it can be seen that for samples with lower spin concentration the difference between T_m and T_2 increases. The concentration dependence predicted by equation (4.11) is observed for the first three points with the lowest concentration. The dashed line shows a fit according to equation (4.11), from which $T_1^B = 63$ ms is calculated. This value is comparable with $T_1^a = 95$ ms for P@C_{60} at this temperature. Therefore it can be assumed that the second hyperfine line of P@C_{60} play the role of B spins in the spectral diffusion. The contribution of instantaneous diffusion to the spin-spin relaxation was tested using the $\pi/2-\tau-\theta$ pulse sequence where θ is the rotation angle of the second MW pulse [111]. T_m should depend on $\sin^2(\theta)$ according to equation (4.12) if instantaneous diffusion makes a strong contribution to the relaxation. $1/T_m$ as a function of $\sin^2(\theta)$ for polycrystalline P@C_{60} is shown in Fig. 4.8. The measured relaxation times are shown together with error bars to highlight that there is no dependence (or a very weak one) of T_m on $\sin^2(\theta)$. This result suggests that instant diffusion does not make a significant contribution to the transverse spin relaxation as expected at this low spin concentration [105].

The spin-spin relaxation of P@C_{60} encapsulated in BrPOT should differ from that of "bulk" P@C_{60}. Due to the small size of the available samples the relaxation

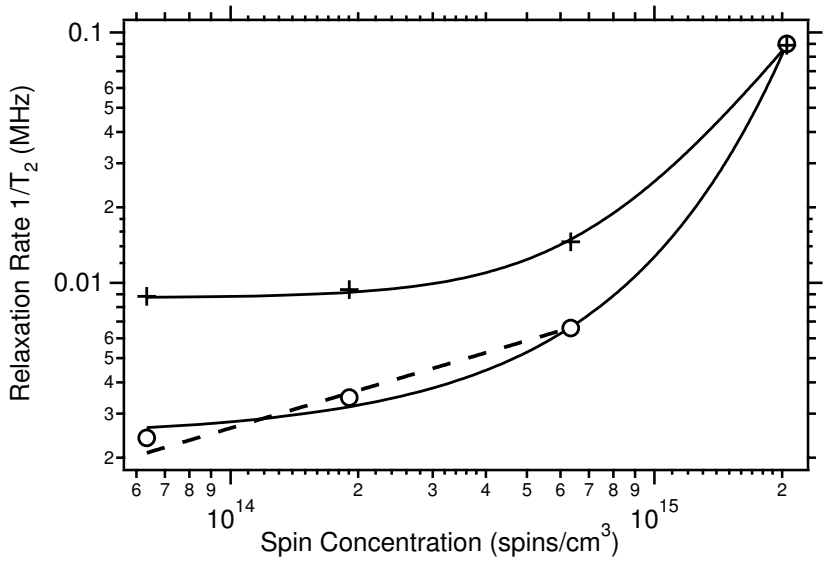

Fig. 4.7: Dependence of the spin-spin relaxation rates on the spin concentration of polycrystalline P@C_{60} measured by ESE decay (crosses) and by the CPMG pulse sequence (circles) at $T = 10$ K. The solid lines are exponential fits $f(c) \sim e^{Bc}$ where c is the spin concentration. The dashed is a fit with $f(c) \sim \sqrt{Bc}$ to the first three points according to equation (4.11).

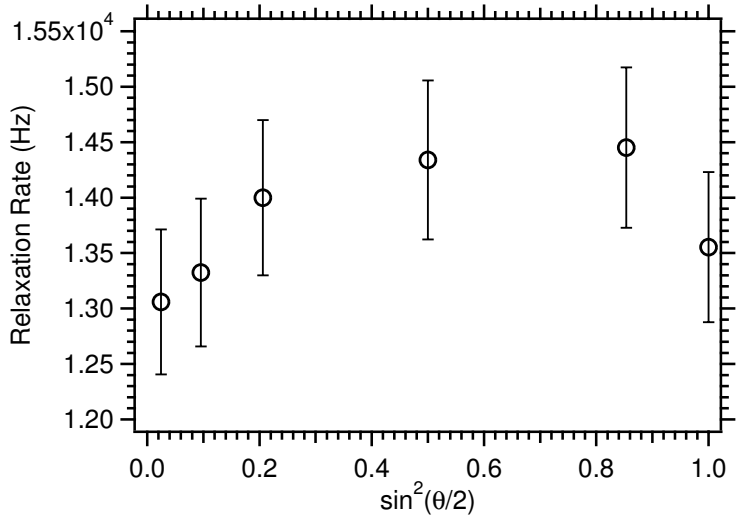

Fig. 4.8: Spin-spin relaxation rate as a function of $\sin^2(\theta/2)$ where θ is the turning angle of the second MW pulse in the Hahn echo sequence.

measurements were performed in W-Band. Thus strictly speaking no direct comparison between the relaxation of the bulk and encapsulated P@C_{60} is possible. The spin concentration of P@C_{60} (m(P@C_{60})/m(C_{60})) used for the production of the BrPOT crystal was about 10^{-4}. In Fig. 4.9 the spin-spin relaxation rate (measured with the Hahn echo pulse sequence) is plotted together with the ZFS parameter as a function of the temperature. It can be seen that generally the

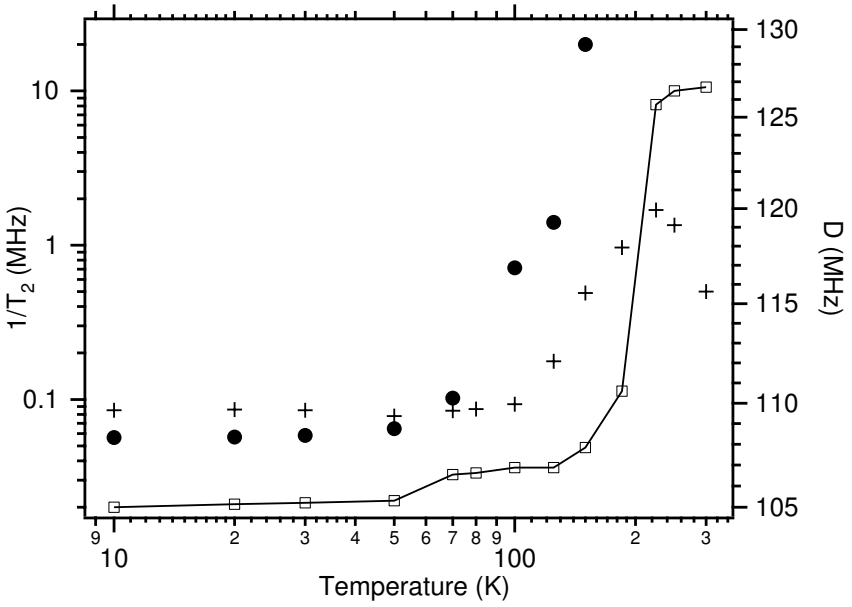

Fig. 4.9: Temperature dependence of the spin-spin relaxation rates of P@C_{60} in rhombohedral BrPOT and of the zero-field splitting parameter D. Crosses denote $1/T_m$ for the transition $m_s = +1/2 \leftrightarrow m_s = -1/2$, circles for the $m_s = +1/2 \leftrightarrow m_s = -3/2$ transition and squares the ZFS. The line connect the data points as a guide to the eye.

absolute values for T_2 at low temperature are of the same order as in polycrystalline P@C_{60}, in contrast to T_1. Since the degeneracy in the electron spin $S = 3/2$ system is lifted, T_m can be selectively measured on each transition corresponding to different elements of the relaxation matrix given in equation (4.2). T_m for the two transitions $m_s = -1/2 \leftrightarrow m_s = -3/2$ and $m_s = +3/2 \leftrightarrow m_s = +1/2$ was found to be equal as expected and will be denoted as $T_m^{3/2}$. For T_m of the $m_S = +1/2 \leftrightarrow m_S = -1/2$ transition the notation $T_m^{1/2}$ will be used. $T_m^{3/2}$ could not be measured from room temperature down to 150 K, where a value of 50 ns was obtained. Detection of smaller $T_m^{3/2}$ is hindered experimentally by the spectrometer dead time. Therefore no Hahn echo could be observed in this temperature region for the $m_s = +1/2 \leftrightarrow m_s = -3/2$ ($m_s = -3/2 \leftrightarrow m_s = +1/2$) transition although the corresponding ESR lines are visible in the CW spectrum. $T_m^{3/2}$ increases with decreasing the temperature and below $T = 50$ K it is constant. The echo decays from 50 K up to 150 K are well described by an exponential function while below 50

K, a fit with $f(2\tau) \sim (2\tau/T_m^{3/2})^2$, where τ is the inter-pulse distance, was used. For the transition with $m_S = +1/2 \leftrightarrow m_S = -1/2$ the same fit function had to be used already at $T = 100$ K. This echo decay function is predicted for systems where the spin-spin relaxation is caused only by pure magnetic dipolar broadening [109, 108]. It seems that this process becomes the most important one at lower temperatures. From Fig. 4.9 it can be clearly seen that $T_m^{3/2} > T_m^{1/2}$, similar to what has been observed in polycrystalline "bulk" P@C_{60} [47]. In the latter $T_m^{1/2}$ was measured by selectively pulsing on the main line (transition $m_S = +1/2 \leftrightarrow m_S = -1/2$) and $T_m^{3/2}$ by selective excitation of the broad satellite lines. A ratio $T_m^{3/2} : T_m^{1/2} = 4 : 3$ was found, where in the encapsulated P@C_{60} the ratio is 3 : 2. The difference in the two relaxation rates suggests that the magnetic dipolar interaction is different for the two transitions.
The rate $1/T_m^{1/2}$ shows a maximum at $T = 225$ K, similar to $1/T_m$ of bulk N@C_{60} (measured at W-Band but the maximum appears at $T = 160$ K) [93, 94]. The latter maximum was ascribed to a resonance between the molecular jump reorientation frequency of the C_{60} cage and the size of the fine structure. This suggestion was supported with ^{13}C NMR [113] data and μSR measurements [114]. These experiments were not performed with BrPOT, so there is no information about the motion of the encapsulated C_{60} molecules. However, the temperature dependence of the size of the zero-field splitting shows a jump at $T \approx 220$ K which can be connected to the maximum of $1/T_m^{1/2}$. This jump of both ZFS and $1/T_m^{1/2}$ at the same temperature indicates a change in the crystal structure. The strong variation of the ZFS is accompanied by larger fluctuations of its mean value which increase the spin-spin relaxation. Thus at temperatures above 50 K, these fluctuations determine the coherence time.

4.4 Conclusions

The transversal spin relaxation of magnetically diluted polycrystalline P@C_{60} has been investigated at $T = 10$ K. Hahn echo and CPMG pulse sequences were used to measure T_m and T_2 respectively. It was found that spectral diffusion is the main relaxation mechanism and not contribution from instant diffusion was found. The longest measured value for T_2 was estimated to be 0.4μs, which corresponds to $N_{gate} = 8000$ if the average gate time is $t_{gate} = 50$ ns.
The spin-lattice relaxation of P@C_{60} in rhombohedral BrPOT has been measured at various temperatures. Two relaxation rates $1/T_1^a$ and $1/T_1^b$ with similar temperature dependence were found. Fluctuations of both hyperfine interaction and ZFS parameters were found to influence the longitudinal relaxation.

The large ZFS in encapsulated P@C_{60} allow the selective excitation of all ESR transition in this spin $S = 3/2$ system in contrast to the bulk P@C_{60}. While $1/T_1$ was found not to depend on the transition, the spin-spin relaxation time T_m is different for transitions involving $|m_S| = 3/2$ than for transition with $|m_S| = 1/2$. The two coherence times $T_m^{3/2}$ and $T_m^{1/2}$ have different temperature dependences. $T_m^{3/2}$ could be measured first at $T = 150$ K and increases with decreasing the temperature and below $T = 50$ K it is longer than $T_m^{1/2}$. The latter shows a sharp minimum at $T = 220$ K where the size of the ZFS changes abruptly. Thus the fluctuations of the ZFS determine the spin-spin relaxation in this temperature regime.